The role of islet lipid composition remodeling in regulation of beta-cell death via ADP-ribosyl-acceptor glycohydrolase ARH3 signaling in insulitis

Ernesto S. Nakayasu[1*], Michelle Guney[2], Jennifer Kyle[1], Dylan Sarbaugh[2], Cailin Dieter[2], Ruichuan Yin[3], Yi Cui[4,5], Carrie Nicora[1], Farooq Syed[6], Jonas Juan Mateu[7,8], Raghavendra Mirmira[9], Carmella Evans-Molina[6], Decio L. Eizirik[7,10], Bobbie-Jo M. Webb-Robertson[1,11], Kristin Burnum-Johnson[4], Galya Orr[4], Julia Laskin[3], Thomas O. Metz[1], Lori Sussel[2], Charles Ansong[1*]

[1]Biological Sciences Division, Pacific Northwest National Laboratory, Richland, WA, USA
[2]Barbara Davis Center for Diabetes, University of Colorado Anschutz Medical Center, Aurora, CO, USA
[3]Department of Chemistry, Purdue University, West Lafayette, IN, USA
[4]Environmental and Molecular Sciences Laboratory, Pacific Northwest National Laboratory, Richland, WA, USA
[5]Media Lab, Massachusetts Institute of Technology, Cambridge, MA, USA
[6]Center for Diabetes and Metabolic Diseases and the Herman B Wells Center for Pediatric Research, Indiana University School of Medicine, Indianapolis, IN, USA
[7]ULB Center for Diabetes Research, Université Libre de Bruxelles (ULB), Brussels, Belgium
[8]Centre for Genomic Regulation (CRG), The Barcelona Institute of Science and Technology, Barcelona, Spain
[9]Kovler Diabetes Center and Department of Medicine, The University of Chicago, Chicago, IL, USA
[10]Indiana Biosciences Research Institute Diabetes Center, Indianapolis, IN, USA
[11]Department of Biostatistics and Informatics, University of Colorado Anschutz Medical Center, Aurora, CO, USA

*Correspondence to Charles Ansong (Email: charles.ansong@pnnl.gov, Phone: +1 (509) 371-6327) and Ernesto S. Nakayasu (Email: ernesto.nakayaus@pnnl.gov, Phone: +1 (509) 371-6708).

Abstract

Lipids have been implicated as mediators of insulitis and β-cell death in type 1 diabetes development, but it is poorly understood how islet lipid profiles are changed in response to the signaling pathways triggered by insulitis. Here, we investigated the changes in islet/β-cell lipid composition using three models of insulitis and type 1 diabetes progression: isolated human islets and EndoC-βH1 β-cells treated with the proinflammatory cytokines IL-1β and IFN-γ, and islets from non-obese diabetic (NOD) mice isolated before the onset of diabetes. Lipidomic analyses of these three models showed a consistent change in abundance of the lysophosphatidylcholine, phosphatidylcholine and triacylglycerol species. Immunohistochemistry and fluorescence in-situ hybridization showed an enrichment of lysophosphatidylcholine biosynthetic enzyme PLA2G6 in mouse islets. These results were consistent with the lipid profiles obtained using mass spectrometry imaging, which showed an enrichment of lysophosphatidylcholine in mouse islets. Furthermore, we determined that the ADP-ribosyl-acceptor glycohydrolase ARH3 is regulated by cytokines downstream of PLA2G6 and that this regulation may represent a negative feedback mechanism that reduces cytokine-induced apoptosis. Overall, these data show the importance of lipid metabolism in regulating β-cell death in type 1 diabetes.

Keywords: Type 1 diabetes, insulitis, lipidomics, phospholipase, poly(ADP)ribosylation, β-cell death

INTRODUCTION

Type 1 diabetes (T1D) affects over 1.25 million people in the U.S. and is characterized by the autoimmune destruction of the insulin-producing β cells of the pancreas (1). This results in the disruption of blood glucose regulation and has deleterious downstream effects to the body, reducing the life expectancy of individuals with T1D by approximately 12 years (2). Currently, the treatment of T1D relies on exogenous insulin administration and there is no cure or permanent remission from the disease. Therefore, there is an urgent need to better understand the mechanisms that contribute to β-cell loss in order to inform the development of novel treatment therapies.

Lipids play major roles in all tissues of the body, being the major structural component of membranes, energy storage molecules and cell-signaling mediators. T1D is associated with changes in serum lipid profiles after disease onset, including increases in blood triacylglycerol and cholesterol levels, which are often associated with poor glycemic control (3). However, limited information is available regarding the roles of lipids in contributing to disease pathogenesis. For instance, the Oresic group found that circulating lipids function as biomarkers for autoimmunity and T1D progression (4; 5). In terms of cell signaling, lipids have been shown to be important mediators of the islet inflammatory process (insulitis) (6-8). During insulitis, pro-inflammatory cytokines activate phospholipases, such as inducible phospholipase A2 (PLA2), leading to the cleavage of phosphatidylcholine (PC) into lysophosphatidylcholine (LPC) (7; 9; 10). This process also leads to the release of fatty acids, such as arachidonic acid, which can be converted into prostaglandins, leukotrienes and thromboxanes that activate pro-apoptotic signaling and contribute to β-cell death (11-13).

At present, the role of the islet lipidome during the progression of T1D is poorly understood. Mass spectrometry analysis of islets has identified LPC and ceramides as important molecules in β-cell death (10). However, the lipidomics coverage in that study was limited and recent advances in technology can provide a more comprehensive coverage of the islet lipidome. Here, we used 3 models of insulitis and type 1 diabetes progression to study the changes in islet/β cell lipid composition during this process. Thus, unbiased lipidomics analyses were performed in 1) human islets and 2) a human β-cell line exposed to the proinflammatory cytokines IL-1β and IFN-γ, and 3) in islets from non-obese diabetic (NOD) mice. The analysis showed a consistent regulation of LPC, PC with long unsaturated fatty acid chains and triacylglycerol species across the different models. To further investigate the LPC regulation, we performed mass spectrometry imaging analysis and microscopy of its biosynthetic enzyme PLA2G6 in mouse islets. The results showed that both LPC and PLA2G6 are enriched in islets. We also investigated the signaling mediated by PLA2G6 in mouse Min6 β cells using RNAi followed by proteomics analysis. This analysis determined that the ADP-ribosyl-acceptor glycohydrolase ARH3 is regulated by cytokines and that this regulation provides a negative feedback mechanism that reduces cytokine-induced apoptosis.

RESEARCH DESIGN AND METHODS

Mice

Female 6-week-old non-obese diabetic NOD/ShiLtJ (#001976) and non-obese diabetes-resistant NOR/LtJ (#002050) mice were purchased from Jackson Labs. Husbandry of mice and experimental procedures were performed according to the University of Colorado approved IACUC protocol #00045. The mice were housed for < 1 week prior to islet isolation. Approximately 320-520 islets (n=3) were isolated using Histopaque centrifugation gradient and further handpicking of islets as described previously (14).

Human pancreatic islet and EndoC-βH1 cells

The lipidomics data of the human islets (n=10) (**Supplementary Table 1**) and EndoC-βH1 cells (n=4) treated with 50 U/mL IL-1β + 1000 U/mL IFN-γ were collected from the same samples of proteomic analyses carried out us in (15) and (16), respectively. Culture maintenance, treatment and harvesting information are described in detail elsewhere (15; 16).

MIN6 β cell line culture and treatment

MIN6 cells were cultured in DMEM containing 10% FBS and 1% penicillin-streptomycin and maintained at 37˚C in 5% CO_2. For knock-down experiments of *PLA2g6* siRNA was obtained from Dharmacon. Cells were transfected using Lipofectamine RNAiMAX (Invitrogen) with SMARTpool ON-TARGETplus non-targeting siRNA or siRNA targeting *PLA2g6* (Dharmacon). For studies using cytokines, cells were treated 24 h after transfection with 100 ng/mL IFN-γ, 10 ng/mL TNF-α, and 5 ng/mL IL-1β for 24 h.

Sample extraction

Samples were subjected to metabolite, protein and lipid extraction (MPLEx) (17). Briefly, cells and islets were suspended in water and extracted by adding 5 volumes of cold (-20 °C) chloroform/methanol solution (2/1, v/v), incubating 5 min on ice and vigorously vortexing. Metabolites, proteins and lipids were separated into different phases by centrifuging the samples for 10 min at 16,000xg at 4°C. Metabolites and lipids were collected into glass autosampler vials and dried in a vacuum centrifuge. Proteins were washed by adding 1 mL of cold (-20°C) methanol and centrifuging 10 min at 16,000xg at 4°C. The supernatant was discarded, and pellets were dried in a vacuum centrifuge. Samples were stored at -80 °C until analysis.

Lipidomic analysis

Extracted lipids were dried and resuspended in methanol before being subjected to LC-MS/MS analysis as previously described in detail (18). Lipid species were identified using LIQUID (18) and manually inspected for validation. The features of the identified lipid species were extracted and aligned using MZmine (19).

Proteomic analysis

Extracted proteins were dissolved in 50 mM NH_4HCO_3 containing 8 M urea and 10 mM dithiothreitol. After incubating for 1 h at 37 ºC with shaking at 800 rpm, 400 mM iodoacetamide was added to a final concentration of 40 mM, and the mixture incubated for another hour in the dark at room temperature. The reaction mixture was 8-folds diluted with 50 mM NH_4HCO_3, and 1 M $CaCl_2$ was added to a final concentration of 1 mM. Proteins were digested for 3 h at 37 ºC using trypsin at 1:50 enzyme:protein ratio. Digested peptides were desalted by solid-phase extraction using C18 cartridges (Discovery, 50 mg, Sulpelco) and dried in a vacuum centrifuge.

Peptides were analyzed on a Waters NanoAquity UPLC system with a custom packed C18 column (70 cm × 75 µm i.d., Phenomenex Jupiter, 3 µm particle size, 300 Å pore size) coupled with a Q-Exactive mass spectrometer (Thermo Fisher Scientific). Peptide separation was carried out with a gradient of water (solvent A) and acetonitrile (solvent B) both containing 0.1% formic acid (1-8% B in 2 min, 8-12% B in 18 min, 12-30% B in 55 min, 30-45% B in 22 min, 45-95% B in 3 min, hold for 5 min in 95% B and 99-1% B in 10 min). Eluting peptides were directly analyzed by nanoelectrospray ionization and full-MS scans were collected at a resolution of 35,000 at 400 *m/z*. The 12 most intense parent ions were submitted to high-energy collision induced dissociation fragmentation with a 30% normalized collision energy.

Data were processed with MaxQuant software (v.1.5.5.1) (20) by matching against the mouse reference proteome database from Uniprot Knowledge Base (downloaded August 14, 2018). Searching parameters included protein N-terminal acetylation and oxidation of methionine as variable modifications, and carbamidomethylation of cysteine residues as fixed modification. Mass shift tolerance was used as the default setting of the software. Only fully tryptic digested peptides were considered, allowing up to two missed cleaved sites per peptide. Quantification of proteins was done using the intensity-based absolute quantification (iBAQ) method (21).

Statistical analysis

The lipidomics data were log2 transformed and subjected to quality control analysis to identify any sample issues via Principal Component Analysis (PCA), robust to missing data for proteomics (22), as well as a robust PCA approach based on the distributional properties of the measured biomolecules for each sample (23). No sample-level issues

were detected and subsequently the lipidomics data were evaluated for total abundance bias and, with none found, were global median centered (24). Given the experimental design, statistics were then performed via a standard paired *t*-test followed by a multiple test Bonferroni correction (25). The proteomics data was log2 transformed, and normalized by linear regression and central tendency using InfernoRDN (former Dante) (26). Statistically significant proteins were determined by ANOVA and *t*-test.

Bioinformatics analysis

The significantly different lipids and proteins were submitted to ontology/function-enrichment analysis using Lipid MiniOn (27) and DAVID (28) tools, respectively. For the Lipid MiniOn analysis, the full list of identified lipids was set as the background and the significantly different species as the query. Ontologies were considered enriched with a $p \leq 0.05$ using the Fisher's exact test. For the DAVID analysis, the differentially abundant proteins were set as the query and the entire genome was set as the background. Only the pathways of the KEGG database were used for the analysis and considered enriched with a $p \leq 0.05$.

Tissue processing and immunohistochemistry

Pancreata were dissected, washed in ice cold PBS, and fixed for 4 hours in 4% PFA at 4 $^{\circ}$C. The tissue was then incubated in 30% sucrose overnight and frozen in OCT. 10 µm cryosections were taken and placed on Superfrost Plus slides (Fisher Scientific). Immunohistochemistry for PLA2G6 was performed using the Mouse on Mouse kit (Vector Labs) and the Vectastain ABC HRP kit (Vector Labs).

Mass spectrometry imaging analysis

Nanospray desorption electrospray ionization (nano-DESI) mass spectrometry imaging was performed on a Q Exactive HF-X mass spectrometer (Thermo Fisher Scientific) as previously described (29). High-resolution nano-DESI probes were assembled using two fused silica capillaries pulled to O.D. 15- 25 µm. A shear force probe with a tip diameter of ~10 µm was integrated with the nano-DESI probe and was used to precisely control the distance between the probe and the sample. The position of the samples was controlled by a motorized XYZ stage. Samples were scanned at a rate of 10 µm/s under the nano-DESI probe in lines with a step of 20 µm between the lines. A 9/1 (v/v) methanol/water mixture containing 200 nM LPC 19:0 (internal standard) was propelled through the nano-DESI probe at 500 nL/min. The instrument was operated in a positive ionization mode with the following parameters: *m/z* range of 150−1000; mass resolution of 60,000 at *m/z* 200; high voltage of 3.2 kV. A custom-designed software, MSI QuickView, was used for data visualization and processing. Ion images were generated by normalizing the signal of the analyte to the signal of the internal standard (LPC 19:0). Lipids were identified by matching based on the high mass accuracy against the species characterized in the lipidomics analysis.

Fluorescence in-situ hybridization (FISH)

FISH experiments were performed as previously described (30). Ten oligonucleotide probes containing targeting and 3' readout overhang domains were designed against the *Pla2g6* transcript coding region (see **Supplementary Table 2** for sequences). Each targeting domain was 20-nt long and complementary to the *Pla2g6* mRNA, with CG content of 40-60%, no self-repeats and inner loop structures. A secondary probe labeled with two Alexa647 molecules was used to hybridize with the 3' overhang domain.

Samples were fixed with fresh 4% paraformaldehyde. After quenching the residual paraformaldehyde was with 0.1% sodium borohydride, samples were permeabilized with 0.2% Triton-X 100 and stored in 70% ethanol. The primary and secondary probes (50 nM final concentration) and anti-insulin antibody (**Supplementary Table 2**) (1000-folds dilution) were diluted in hybridization solution (10% dextran sulfate, 15% formamide, 1× SSC, 3.4 mg/mL tRNA, 0.2 mg/mL RNase-free BSA, 2 mM ribonucleoside vanadyl complex) and incubated with the samples 37°C overnight in a humid chamber. Samples were rinsed with 15% formamide in 1× SSC, followed by staining with Atto 488-conjugated secondary antibody (**Supplementary Table 2**) and DAPI. Images were collected on an Olympus IX71-based single-molecule microscope equipped with 405 nm, 488 nm, and 640 nm solid lasers. Images were captured using a 100× oil immersion objective lens (NA 1.4) and an EMCCD camera (Andor iXon Ultra 897). Fluctuation localization imaging-based FISH (fliFISH) was used to extract the true location of *pla2g6* mRNA in tissue sections to account for the background noise (30). The location for each *Pla2g6* transcript was so calculated based on the center of mass. Photoswitching was activated by using GLOX-containing buffer: 50 mM Tris, 10 mM NaCl, 10% glucose, 560 µg/mL glucose oxidase, 34 µg/mL catalase and 1% β-mercaptoethanol.

Quantitative real-time PCR analysis

Cells were harvested and total mRNA was extracted using the RNeasy Mini kit (Qiagen). cDNA synthesis was performed using the iScript synthesis kit (Biorad) and qRT-PCR assays were performed using SsoAdvanced Universal SYBR Green Supermix. Expression levels were normalized to the housekeeping gene GAPDH and quantified using the delta CT method (see **Supplementary Table 2** for oligonucleotide information).

Western Blotting

Cells were harvested in RIPA buffer containing protease inhibitors and proteins were electrophoresed and transferred to PVDF membranes. After blocking in 5% milk in TBS containing 0.1% Tween 20, membranes were incubated in specific primary antibodies at 4˚ C overnight. Anti-mouse and anti-rabbit horseradish peroxidase-conjugated antibodies (**Supplementary Table 2**) were used for secondary antibodies and enhanced chemiluminescent substrate was used for signal detection.

RESULTS

Lipidome analysis of β-cell death/type 1 diabetes models

We performed comprehensive lipidomic analysis of three models of β-cell death in T1D: (I) Human EndoC-βH1 cells exposed to the cytokines IL-1β + INF-γ for 48 h, (II) human islets exposed to the same cytokines for 24 h, and (III) islets from non-obese diabetic (NOD) mice at the pre-diabetic stage (6-week old) vs. age-matched NOR mice. A total of 369, 558 and 251 lipid species were identified and quantified in EndoC-βH1 cells, human islets and murine islets, respectively (**Figure 1A, Supplementary Tables 3-8**). A striking difference in the number of lysophospholipid species were observed comparing EndoC-βH1 cells with human or murine islets. Only 9 (2.4% of the total) lysophospholipid species were detected in EndoC-βH1 cells, compared to 89 (15.9%) and 25 (10.0%) in human and murine islets, respectively. To better understand possible lipid metabolic processes regulated in each of the models, we performed an enrichment analysis using Lipid Mini-On (27). This tool determines whether any specific lipid feature, such as head group, subclass, fatty acyl chain length or degree of unsaturation, is

overrepresented among the differentially regulated lipids. In EndoC-βH1 cells, phosphatidylglycerol (PG), plasmanyl-phosphatidylethanolamine and lipids with polyunsaturated fatty acyl chains were enriched among the species regulated by the IL-1β + INF-γ treatment (**Figure 1B**). Similarly, lipids with polyunsaturated fatty acyl chains were also enriched in human islets treated with the cytokines (**Figure 1B**). In murine islets, only triacylglycerols (TG) with 58 total carbons in the fatty acyl chains were found to be significantly enriched (**Figure 1B**).

We reasoned that lipid groups regulated in a coordinated/common fashion in EndoC-βH1 cells, human islets, and murine islets in response to proinflammatory cytokines were likely to be important for T1D pathogenesis (highlighted by stars in **Figure 1A**). Interestingly, LPC species, PC species with long, polyunsaturated fatty acyl chains, and TGs were commonly regulated across all three models; LPCs and PCs with long, polyunsaturated fatty acids were also upregulated, whereas TGs were consistently downregulated in all 3 sample types (**Figure 2**).

Spatial distribution of coordinately regulated lipids in islets

We further surmised that coordinately regulated lipids that were particularly important for T1D pathogenesis would be preferentially localized to islets. To test this hypothesis, we determined the spatial distribution of the commonly regulated lipid species in murine pancreas using mass spectrometry imaging (MSI). MSI analysis showed that several LPC species are preferentially localized to islets, including LPC(18:0), LPC(18:1) and LPC(20:4), whereas species such as LPC (18:2) and PC(16:0) had similar abundance compared to surrounding tissue **(Figure 3**). In contrast, the standard LPC(19:0), which is delivered with the extraction solvent, was evenly distributed

throughout the tissue (**Figure 3**). Similarly, the endogenous metabolite glycerophosphocholine (GPC) was also evenly distributed throughout the tissue (**Figure 3**), which indicates an insignificant matrix effect (31). As expected, Several PC species including PC(34:1) and PC(36:2) displayed an even distribution between the islets and the surrounding tissue (**Figure 3**). Conversely, species with longer and polyunsaturated fatty acyl chains PC(40:5) and PC(40:6) were clearly enriched in islets (**Figure 3**). Unfortunately, the solvent composition used in imaging experiments did not allow us to analyze TG localization, due to inefficient extraction of this lipid class into 9:1 methanol:water mixture.

LPCs are generated by the release of fatty acid chains from phospholipids, a reaction catalyzed by the enzyme calcium-independent phospholipase A2 (iPLA2b/PLA2G6). Consistent with the localization of LPCs to the human islets, *Pla2g6* was also specifically expressed in β cells in murine islet tissue, as demonstrated by combining fluorescent in situ hybridization (FISH) and immunohistochemistry (**Figure 4A-B**). Taken together these data support the notion that the generation of LPCs by *Pla2g6* is preferentially localized to pancreatic islets and β cells.

Pla2g6-dependent cytokine regulation in MIN6 cells

To begin to understand the molecular mechanism(s) underlying phospholipase PLA2G6-mediated signaling in cytokine-exposed islets, we treated wild-type and *Pla2g6* knockdown (KD) MIN6 β cells with IL-1β + INF-γ + TNFα for 24h, followed by LC-MS/MS-based proteomics analysis. The cytokine treatment led to changes in abundance of 1043 out of the 5212 identified and quantified proteins (**Figure 5A, Supplementary Table 9**). A function-enrichment analysis of the differentially regulated proteins revealed that 52

KEGG pathways were regulated by the cytokine treatment (**Figure 5B**). Only a small fraction of 35 proteins that were differentially regulated by cytokines was dependent on PLA2G6 (**Figure 5C, Supplementary Table 10**). Among these proteins, the expression of cathepsin Z and cathepsin B were upregulated with the cytokine treatment, but this increase in abundance was abolished in the absence of PLA2G6 (**Figures 5D and 5E**). Cathepsins are markers of lysosomal function and autophagy, indicating a possible link between cytokine signaling and these processes through PLA2G6. This is consistent with the previously described role of PLA2G6in the regulation of autophagy and apoptosis in murine islets treated with the ER stressor, thapsigargin (32). Overall, the analysis showed a strong regulation of the MIN6 β cell proteome by pro-inflammatory cytokines, of which a small subset was dependent of PLA2G6.

Regulation of poly(ADP)ribosylation proteins in MIN6 β cells

Among the PLA2G6-dependent cytokine-regulated proteins as judged by LC-MS proteomics was ADP-ribosy-acceptor glycohydrolase ARH3 (ADPRHL2 gene) (**Figure 5C**). ARH3 has been shown to play a role in poly-ADP-ribose (PAR) metabolism, a factor that regulates β-cell death in mice (33). We investigated the abundance profiles of the PAR polymerases (PARP) and hydrolases PAR glycohydrolases (PARG), MacroD1, MacroD2, terminal ADP-ribose protein glycohydrolase 1 (TARG1) and ADP-ribosyl-acceptor hydrolases (ARHs) in the proteomic analysis. PARP-1 abundance decreased approximately 35% in both wild-type and *Pla2g6*-KD cells when treated with cytokines, whereas PARP-2 was not significantly changed (**Table 1**). Conversely, PARP-3, -9, -10, -12 and -14 were strongly upregulated (>5 fold) when cells were treated with cytokines in both wild-type and *Pla2g6*-KD cells (**Table 1**). The PAR hydrolases ARH3 and MacroD1

were also increased by 66% and 31%, respectively, in the wild-type cells treated with cytokines, but their expression was unchanged in *Pla2g6*-KD cells treated with cytokines (**Table 1**). The other PAR hydrolases were not detected in our analysis.

To further investigate the role of ARH3 in β cell stress, we tested the effects of ARH3 KD in cytokine-mediated apoptosis by performing western blots of the apoptotic marker cleaved caspase 3. The KD reduced ARH3 transcript levels by approximately 50% (**Figure 6A**), but to smaller decrease in protein level was observed by western blot (**Figure 6B**) perhaps due to differences in sensitivity between the assays. As expected, the cytokine cocktail IL-1β + INF-γ + TNFα increased the abundance of cleaved caspase 3 by 67%; however, this increase was only 33% in the ARH3 KD cells (**Figure 6A-C**). Together, these data show a strong regulation of the poly(ADP)ribosylation machinery by cytokines in MIN6 β cells and suggest that ARH3 is further regulated by PLA2G6 for protecting β cells from apoptosis during T1D.

DISCUSSION

We presently investigated the remodeling of islet and β cell lipid composition in 3 models of T1D. Since phenotypes found in model systems do not always reflect the physiology of disease, we performed lipidomic analysis across three different models type 1 diabetes: EndoC-βH1 cells exposed to the cytokines IL-1β + INF-γ, human islets exposed to the same cytokines and islets from non-obese diabetic (NOD) mice at the pre-diabetic stage. This analysis identified consistent changes in composition of specific classes of lipids: down regulation of TGs and upregulation of LPCs and PCs with long unsaturated fatty acid chains. TGs have been shown to be down-regulated in rat β cells

by the pro-inflammatory cytokine combination IL-1β + INF-γ + TNFα, likely to accommodate the resulting increased energetic demands (34). TG metabolism has also been associated with cellular protection; it has been shown that GDF15 impairs inflammation-induced damage by systemic release of liver TGs (35). Consistently, TG-carrying protein apolipoprotein CIII reduces apoptosis in rodent β cells treated with IL-1β + INF-γ (36). Also, increases in cellular TG content has been associated with protection of rat β cells against the cytotoxic effects of saturated free fatty acids (37).

Our three different models of T1D also showed a consistent upregulation in the levels of PCs with long polyunsaturated fatty acid chains. Like TGs, polyunsaturated fatty acids have been associated with protection of β cells against pro-inflammatory cytokines (38). An omega 3 polyunsaturated fatty acid diet reduces the incidence of diabetes in NOD mice (39). Polyunsaturated fatty acids are sources for immunomediators such as prostaglandins, leukotrienes and thromboxanes. While some of these immunomediators are anti-inflammatory, others induce inflammation and apoptosis. For instance, the processing of the polyunsaturated fatty acid arachidonic acid into 12-HETE by 12-lipoxygenase has been shown to lead to β-cell death (40).

Polyunsaturated fatty acids are often associated with phospholipids but can be released from them by phospholipases. Cytokines activate the inducible phospholipase A2 beta (iPLA2b/PLA2G6) in islets leading to the release of polyunsaturated fatty acids and LPCs (10; 41). This is in line with our results showing an accordant increase of LPCs in each of the T1D models. We also showed that several LPCs are enriched in islets, which is consistent with the observation that PLA2G6 expression is higher in islets compared to surrounding tissue. A few LPC species were not enriched in islets, which

might be due to the enzyme specificity. In murine islets, PLA2G6 appears to be concentrated in β cells, which is consistent to the previous report showing that its transcript is higher in β cells compared to α cells (42). PLA2G6 has been shown to activate apoptosis via downstream activation of neutral sphingomyelinase and formation of ceramides, leading to mitochondrial membrane decompensation (10). Pharmacological inhibition of PLA2G6 protects NOD mice from developing diabetes (7). PLA2G6 can also induce alternative splicing and reduce the levels of the antiapoptotic protein Bcl-x(L) via neutral sphingomyelinase activation and ER stress (9). In addition, PLA2G6 was previously shown to regulate autophagy and apoptosis in murine islets treated with the ER stressor, thapsigargin (32). This observation agrees with our proteomics data, which shows PLA2G6 regulate lysosomal trafficking and autophagy markers cathepsin B and Z. Of note, another cathepsin, cathepsin H, is a candidate gene for type 1 diabetes with a key role for β-cell function and survival (43) and crinosomes, a cell structure that plays a key role for the generation of autoimmune peptides in diabetes prone NOD-mice (44), are rich in cathepsins.

Here we show that PLA2G6 also regulates antiapoptotic signals by inducing the expression of the ADP-ribosy-acceptor glycohydrolase ARH3. ARH3 hydrolyses PAR from serine residues, counterbalancing the pro-apoptotic activity induced by ADP-ribose polymerization (45-47). Indeed, PARP-1 has been shown to be involved in cytokine mediated β-cell death in murine islets and PARP-1 deletion has been shown to protect against streptozotocin-mediated diabetes (33; 48; 49). Our data show that this scenario might be more complex as PARP-3, -9, -10, -12 and -14 are strongly upregulated in cells

treated with the cytokines IL-1β + INF-γ + TNFα, but their role in β-cell death still needs to be investigated.

Overall, our data showed a consistent regulation of the lipid metabolism in 3 different models of insulitis. Additionally, we demonstrated that phospholipase Pla2g6 signaling leads to the upregulation of ARH3 which may provide a feedback mechanism to reduce apoptosis.

Acknowledgements

The authors thank the NIDDK-supported Integrated Islet Distribution Program (IIDP) for providing the human islets used in the study. Work was performed in the Environmental Molecular Sciences Laboratory, a U.S. Department of Energy (DOE) national scientific user facility at Pacific Northwest National Laboratory (PNNL) in Richland, WA. Battelle operates PNNL for the DOE under contract DE-AC05-76RLO01830.

Funding

This work was supported by National Institutes of Health, National Institute of Diabetes and Digestive and Kidney Diseases grants UC4 DK108101 (to C.A. and L.S.), UC4 DK104166 (to R.G.M, C.E. M., D.L.E, and T.O.M.), R01 DK105588 (to R.G.M.) and R01 DK093954 (to C.E.M); VA Merit Award I01BX001733 (to C.E.M.); Fonds National de la Recherche Scientifique (FNRS), Welbio CR-2015A-06, Belgium (to D.L.E.); a JDRF Strategic Research Agreement (to C.E.M and R.G.M.) and gifts from the Sigma Beta Sorority, the Ball Brothers Foundation, the George and Frances Ball Foundation, and the Holiday Management Foundation (to C.E.M and R.G.M.). F.S. was supported by JDRF postdoctoral fellowship (3-PDF-2016-199-A-N). D.L.E. also received funds from Innovative Medicines Initiative 2 Joint Undertaking under grant agreement No 115797 (INNODIA), which is supported by the Union's Horizon 2020 research and innovation program and EFPIA, JDRF and The Leona M. and Harry B. Helmsley Charitable Trust.

Competing interests

The authors declare that they have no competing interests.

Authors' contributions

E.S.N., L.S., C.A. conceived the study and participated in the study design. E.S.N., M.G., J.K., D.S., C.D., R.Y., Y.C., C.N., F.S., and J.J.M. performed the experiments. All the authors performed the data analysis. E.S.N., R.Y., Y.C., B.J.W.R., J.L., L.S. and C.A. wrote the manuscript. All authors read, revised and approved the final manuscript for publication. C.A. is the guarantor of this work and, as such, had full access to all the data

in the study and takes responsibility for the integrity of the data and the accuracy of the data analysis.

Data and Resource Availability

Proteomics data were deposited into Pride repository (50) (www.ebi.ac.uk/pride) under accession number PXD017863.
Reviewer account details:
Username: reviewer04836@ebi.ac.uk
Password: B4o1VcPd

Table 1 – Abundance profiles of poly(ADP)ribosylation proteins in wild-type and Pla2g6 knockdown MIN6 β cells treated with the pro-inflammatory cytokines. *iBAQ – intensity-based absolute quantification. Statistical test was done with *t*-test considering equal variation and distribution.

		Average iBAQ intensity				Standard deviation							
		Wild type		Pla2g6 RNAi		Wild type		Pla2g6-RNAi		Fold change (Treated/Control)		p-value (Control vs. treated)	
Accession number	Protein	Control	Treated	Control	Treated	Control	Treated	Control	Treated	Wild type	Pla2g6 RNAi	Wild type	Pla2g6 RNAi
Q921K2	PARP-1	160541298	102181010	162185126	98199854	14415018	13769483	11315442	11911652	0.64	0.61	0.000	0.000
O88554	PARP-2	2320187	1886698	2701832	1904552	773539	900914	606622	619003	0.81	0.70	0.438	0.074
Q8CFB8	PARP-3	0	2440297	129711	2796473	0	1950741	290043	1320074	∞	21.56	0.023	0.002
Q8CAS9	PARP-9	1027221	39521623	1758362	44078979	833995	6228610	1232660	4239980	38.47	25.07	0.000	0.000
Q8CIE4	PARP-10	100029	4173449	93000	4561784	223672	1064209	207955	1039258	41.72	49.05	0.000	0.000
Q8BZ20	PARP-12	613429	3541763	861360	6368375	261033	682862	471954	1427301	5.77	7.39	0.000	0.000
Q2EMV9	PARP-14	616310	26623139	769444	27348827	84838	2863548	321341	1432066	43.20	35.54	0.000	0.000
Q8CG72	ARH3	11541195	19182811	11421375	12104702	3610258	2655778	3105854	1940956	1.66	1.06	0.005	0.688
Q922B1	MacroD1	16322818	21400784	19062601	17347089	3285980	2286317	3446722	3884448	1.31	0.91	0.022	0.481

Legends:

Figure 1. Global lipidomic analysis of 3 common models used for the study of β-cell death in type 1 diabetes: (I) EndoC-βH1 cells exposed to IL-1β and INF-γ for 48 h (4 replicates), (II) human islets exposed to same cytokines for 24 h (10 replicates) and (III) islets from non-obese diabetic (NOD) mice in pre-diabetic stage (6 weeks of age) vs. age-matched NOR mice (3 replicates). Lipids were extracted and analyzed by liquid chromatography-tandem mass spectrometry. (A) Number of identified and regulated species in lipid subclass. (B) Lipid features and groups that were significantly enriched ($p \leq 0.05$, Fisher's exact test) among the differentially regulated species. *Lipid classes consistently regulated in all three samples.

Figure 2. Lipid species that are consistently regulated in 3 models of β-cell death in type 1 diabetes. Lipids from EndoC-βH1 cells treated with IL-1β and INF-γ for 48 h, human islets treated with the proinflammatory cytokines IL-1β and INF-γ for 24 h and islets from non-obese diabetic (NOD) mice in pre-diabetic stage (6 weeks of age) were extracted and analyzed by liquid chromatography tandem mass spectrometry. Each lipid species is named with the abbreviation of its class (e.g. LPC and PC) followed by the length of the fatty acid and number of double bounds (separated by colon) in parenthesis. The letters after the lipid names represent different isomers that are separated in the chromatography. The relative abundance in T1D model vs. control are color-coded. Isobaric coeluting species (separated by semicolons) were co-quantified.

Figure 3. Spatial localization of lysophosphatidylcholine (LPC) and phosphatidylcholine (PC) species in pancreata from NOR mice by mass spectrometry imaging. Each panel shows either the optical image or color-coded distribution of different lipid, endogenous metabolite [glycerophosphocoline (GPC)] and standard [LPC(19:0)] species. Each lipid species is named with the abbreviation of its class (e.g. LPC and PC) followed by the length of the fatty acid chains and number of double bounds (separated by colon) in parenthesis. Pancreata from 6-week old mice were collected and analyzed in two independent experiments.

Figure 4. Pla2g6 distribution. (A) Fluorescence in situ hybridization (FISH) of MIN6 β cell line, and pancreata from non-obese diabetic (NOD) and non-obese diabetes resistant (NOR) mice (6 weeks of age). Cells and tissues were stained with anti-insulin antibody (green), DNA stain 4′,6-diamidino-2-phenylindole (DAPI – blue) and fluorescent-labeled antisense Pla2g6 oligonucleotide (red). (B) Immunohistochemistry (IHC) analysis of Pla2g6. Tissue was stained with biotin-conjugated anti-Pla2g6 antibodies followed by avidin-conjugated horseradish peroxidase. Localization was visualized by horseradish peroxidase-mediated oxidation and precipitation of 3,3′-diaminobenzidine (brown).

Figure 5. Pro-inflammatory cytokines IL-1β + IFN-γ + TNFα and Pla2g6-dependent proteome remodeling in MIN6 β cells. (A) Pro-inflammatory cytokines (Cyt)-dependent protein expression in wild-type (WT) and Pla2g6-RNAi MIN6 cells (n=5, each). (B) KEGG pathways enriched with proteins differentially abundant in IL-1β + IFN-γ-treated MIN6 cells. Pathways were grouped based on shared proteins using Enrichment Map (51). Each pathway is represented by a node and their degree of connectivity (thickness of the edges) is proportional to the number of shared proteins between the pathways. (C) Pla2g6-dependent protein abundance changes of pro-inflammatory cytokine-treated MIN6 cells. (D-E) Abundance profiles of cathepsin Z (D) and B (E). Statistical test: ** $p \leq 0.01$ and *** $p \leq 0.001$ by *t*-test considering equal distribution and variance.

Figure 6. The role of ADP-ribosy-acceptor glycohydrolase ARH3 in cytokine-mediated apoptosis of MIN 6 β cells. MIN6 cells were transfected with ARH3 RNAi or scrambled oligonucleotides for 24 h and then treated with 100 ng/mL IFN-γ, 10 ng/mL TNF-α, and 5 ng/mL IL-1β for another 24 h. (A) Quantitative PCR of ARH3 transcript normalized by GAPDH. (B) Western blot analysis of ARH3 KD cells treated with cytokines. (C) Quantification of the levels of cleaved caspase 3 bands. The data is representative of 3 independent experiments with similar results.

Supplementary Material

Supplementary table 1 - Characteristics of human islet donors.

Supplementary table 2- List of antibodies and oligonucleotides used in the study.

Supplementary table 3 - Quantitative lipidomics analysis in the negative-ionization mode of the EndoC-βH1 cells (n=4) treated with 50 U/mL IL-1β + 1000 U/mL IFN-γ for 48 h.

Supplementary table 4 - Quantitative lipidomics analysis in the positive-ionization mode of the EndoC-βH1 cells (n=4) treated with 50 U/mL IL-1β + 1000 U/mL IFN-γ for 48 h.

Supplementary table 5 - Quantitative lipidomics analysis in the negative-ionization mode of the human islets (n=10) treated with 50 U/mL IL-1β + 1000 U/mL IFN-γ for 24 h.

Supplementary table 6 - Quantitative lipidomics analysis in the positive-ionization mode of the human islets (n=10) treated with 50 U/mL IL-1β + 1000 U/mL IFN-γ for 24 h.

Supplementary table 7 - Quantitative lipidomics analysis in the negative-ionization mode of islets from 6-weeks old NOD vs NOR mice.

Supplementary table 8 - Quantitative lipidomics analysis in the positive-ionization mode of islets from 6-weeks old NOD vs NOR mice.

Supplementary table 9 - Quantitative proteomics analysis of wild-type and Pla2g6 knock down MIN6 β cells treated with cytokines (100 ng/mL IFN-γ, 10 ng/mL TNF-α, and 5 ng/mL IL-1β) for 24 h.

Supplementary table 10 - Identification of proteins that the abundances are regulated by cytokines via PLA2G6. Wild-type and Pla2g6 knock down MIN6 β cells treated with cytokines (100 ng/mL IFN-γ, 10 ng/mL TNF-α, and 5 ng/mL IL-1β) for 24 h were analyzed by proteomics. The criteria for selecting as PLA2G6-dependent cytokine regulated proteins were: (i) significantly regulated regulated by the cytokine treatment (untreated wild type vs. wild type treated with cytokines), (ii) this regulation also had to be significant comparing wild type treated with cytokines vs. Pla2g6 knockdown treated with cytokines, and (iii) not significantly changing in untreated Pla2g6 knockdown vs. Pla2g6 knockdown treated with cytokines.

References

1. DiMeglio LA, Evans-Molina C, Oram RA: Type 1 diabetes. Lancet 2018;391:2449-2462
2. Huo L, Harding JL, Peeters A, Shaw JE, Magliano DJ: Life expectancy of type 1 diabetic patients during 1997-2010: a national Australian registry-based cohort study. Diabetologia 2016;59:1177-1185
3. Verges B: Lipid disorders in type 1 diabetes. Diabetes Metab 2009;35:353-360
4. Lamichhane S, Ahonen L, Dyrlund TS, Kemppainen E, Siljander H, Hyoty H, Ilonen J, Toppari J, Veijola R, Hyotylainen T, Knip M, Oresic M: Dynamics of Plasma Lipidome in Progression to Islet Autoimmunity and Type 1 Diabetes - Type 1 Diabetes Prediction and Prevention Study (DIPP). Sci Rep 2018;8:10635
5. Oresic M, Gopalacharyulu P, Mykkanen J, Lietzen N, Makinen M, Nygren H, Simell S, Simell V, Hyoty H, Veijola R, Ilonen J, Sysi-Aho M, Knip M, Hyotylainen T, Simell O: Cord serum lipidome in prediction of islet autoimmunity and type 1 diabetes. Diabetes 2013;62:3268-3274
6. Syed I, Rubin de Celis MF, Mohan JF, Moraes-Vieira PM, Vijayakumar A, Nelson AT, Siegel D, Saghatelian A, Mathis D, Kahn BB: PAHSAs attenuate immune responses and promote beta cell survival in autoimmune diabetic mice. J Clin Invest 2019;129:3717-3731
7. Bone RN, Gai Y, Magrioti V, Kokotou MG, Ali T, Lei X, Tse HM, Kokotos G, Ramanadham S: Inhibition of Ca2+-independent phospholipase A2beta (iPLA2beta) ameliorates islet infiltration and incidence of diabetes in NOD mice. Diabetes 2015;64:541-554
8. Dobrian AD, Morris MA, Taylor-Fishwick DA, Holman TR, Imai Y, Mirmira RG, Nadler JL: Role of the 12-lipoxygenase pathway in diabetes pathogenesis and complications. Pharmacol Ther 2019;195:100-110
9. Barbour SE, Nguyen PT, Park M, Emani B, Lei X, Kambalapalli M, Shultz JC, Wijesinghe D, Chalfant CE, Ramanadham S: Group VIA Phospholipase A2 (iPLA2beta) Modulates Bcl-x 5'-Splice Site Selection and Suppresses Anti-apoptotic Bcl-x(L) in beta-Cells. J Biol Chem 2015;290:11021-11031
10. Lei X, Bone RN, Ali T, Zhang S, Bohrer A, Tse HM, Bidasee KR, Ramanadham S: Evidence of contribution of iPLA2beta-mediated events during islet beta-cell apoptosis due to proinflammatory cytokines suggests a role for iPLA2beta in T1D development. Endocrinology 2014;155:3352-3364
11. Ramanadham S, Hsu FF, Bohrer A, Ma Z, Turk J: Studies of the role of group VI phospholipase A2 in fatty acid incorporation, phospholipid remodeling, lysophosphatidylcholine generation, and secretagogue-induced arachidonic acid release in pancreatic islets and insulinoma cells. J Biol Chem 1999;274:13915-13927
12. Ma Z, Ramanadham S, Corbett JA, Bohrer A, Gross RW, McDaniel ML, Turk J: Interleukin-1 enhances pancreatic islet arachidonic acid 12-lipoxygenase product generation by increasing substrate availability through a nitric oxide-dependent mechanism. J Biol Chem 1996;271:1029-1042
13. Chambers KT, Weber SM, Corbett JA: PGJ2-stimulated beta-cell apoptosis is associated with prolonged UPR activation. Am J Physiol Endocrinol Metab 2007;292:E1052-1061
14. Beilke JN, Kuhl NR, Van Kaer L, Gill RG: NK cells promote islet allograft tolerance via a perforin-dependent mechanism. Nat Med 2005;11:1059-1065

15. Nakayasu ES, Syed F, Tersey SA, Gritsenko MA, Mitchell HD, Chan CY, Dirice E, Turatsinze JV, Cui Y, Kulkarni RN, Eizirik DL, Qian WJ, Webb-Robertson BM, Evans-Molina C, Mirmira RG, Metz TO: Comprehensive Proteomics Analysis of Stressed Human Islets Identifies GDF15 as a Target for Type 1 Diabetes Intervention. Cell Metab 2020;
16. Ramos-Rodriguez M, Raurell-Vila H, Colli ML, Alvelos MI, Subirana-Granes M, Juan-Mateu J, Norris R, Turatsinze JV, Nakayasu ES, Webb-Robertson BM, Inshaw JRJ, Marchetti P, Piemonti L, Esteller M, Todd JA, Metz TO, Eizirik DL, Pasquali L: The impact of proinflammatory cytokines on the beta-cell regulatory landscape provides insights into the genetics of type 1 diabetes. Nat Genet 2019;51:1588-1595
17. Nakayasu ES, Nicora CD, Sims AC, Burnum-Johnson KE, Kim YM, Kyle JE, Matzke MM, Shukla AK, Chu RK, Schepmoes AA, Jacobs JM, Baric RS, Webb-Robertson BJ, Smith RD, Metz TO: MPLEx: a Robust and Universal Protocol for Single-Sample Integrative Proteomic, Metabolomic, and Lipidomic Analyses. mSystems 2016;1
18. Dautel SE, Kyle JE, Clair G, Sontag RL, Weitz KK, Shukla AK, Nguyen SN, Kim YM, Zink EM, Luders T, Frevert CW, Gharib SA, Laskin J, Carson JP, Metz TO, Corley RA, Ansong C: Lipidomics reveals dramatic lipid compositional changes in the maturing postnatal lung. Sci Rep 2017;7:40555
19. Pluskal T, Castillo S, Villar-Briones A, Oresic M: MZmine 2: modular framework for processing, visualizing, and analyzing mass spectrometry-based molecular profile data. BMC Bioinformatics 2010;11:395
20. Cox J, Mann M: MaxQuant enables high peptide identification rates, individualized p.p.b.-range mass accuracies and proteome-wide protein quantification. Nat Biotechnol 2008;26:1367-1372
21. Schwanhausser B, Busse D, Li N, Dittmar G, Schuchhardt J, Wolf J, Chen W, Selbach M: Global quantification of mammalian gene expression control. Nature 2011;473:337-342
22. Webb-Robertson BJ, Matzke MM, Metz TO, McDermott JE, Walker H, Rodland KD, Pounds JG, Waters KM: Sequential projection pursuit principal component analysis--dealing with missing data associated with new -omics technologies. Biotechniques 2013;54:165-168
23. Matzke MM, Waters KM, Metz TO, Jacobs JM, Sims AC, Baric RS, Pounds JG, Webb-Robertson BJ: Improved quality control processing of peptide-centric LC-MS proteomics data. Bioinformatics 2011;27:2866-2872
24. Webb-Robertson BJ, Matzke MM, Jacobs JM, Pounds JG, Waters KM: A statistical selection strategy for normalization procedures in LC-MS proteomics experiments through dataset-dependent ranking of normalization scaling factors. Proteomics 2011;11:4736-4741
25. Assennato G, Bruzzi P: [Bonferroni in biomedical research]. G Ital Nefrol 2002;19:178-183
26. Polpitiya AD, Qian WJ, Jaitly N, Petyuk VA, Adkins JN, Camp DG, 2nd, Anderson GA, Smith RD: DAnTE: a statistical tool for quantitative analysis of -omics data. Bioinformatics 2008;24:1556-1558
27. Clair G, Reehl S, Stratton KG, Monroe ME, Tfaily MM, Ansong C, Kyle JE: Lipid Mini-On: mining and ontology tool for enrichment analysis of lipidomic data. Bioinformatics 2019;35:4507-4508

28. Huang da W, Sherman BT, Lempicki RA: Systematic and integrative analysis of large gene lists using DAVID bioinformatics resources. Nat Protoc 2009;4:44-57
29. Yin R, Burnum-Johnson KE, Sun X, Dey SK, Laskin J: High spatial resolution imaging of biological tissues using nanospray desorption electrospray ionization mass spectrometry. Nat Protoc 2019;14:3445-3470
30. Cui Y, Hu D, Markillie LM, Chrisler WB, Gaffrey MJ, Ansong C, Sussel L, Orr G: Fluctuation localization imaging-based fluorescence in situ hybridization (fliFISH) for accurate detection and counting of RNA copies in single cells. Nucleic Acids Res 2018;46:e7
31. Lanekoff I, Stevens SL, Stenzel-Poore MP, Laskin J: Matrix effects in biological mass spectrometry imaging: identification and compensation. Analyst 2014;139:3528-3532
32. Lei X, Bone RN, Ali T, Wohltmann M, Gai Y, Goodwin KJ, Bohrer AE, Turk J, Ramanadham S: Genetic modulation of islet beta-cell iPLA(2)beta expression provides evidence for its impact on beta-cell apoptosis and autophagy. Islets 2013;5:29-44
33. Andreone T, Meares GP, Hughes KJ, Hansen PA, Corbett JA: Cytokine-mediated beta-cell damage in PARP-1-deficient islets. Am J Physiol Endocrinol Metab 2012;303:E172-179
34. Kiely A, McClenaghan NH, Flatt PR, Newsholme P: Pro-inflammatory cytokines increase glucose, alanine and triacylglycerol utilization but inhibit insulin secretion in a clonal pancreatic beta-cell line. J Endocrinol 2007;195:113-123
35. Luan HH, Wang A, Hilliard BK, Carvalho F, Rosen CE, Ahasic AM, Herzog EL, Kang I, Pisani MA, Yu S, Zhang C, Ring AM, Young LH, Medzhitov R: GDF15 Is an Inflammation-Induced Central Mediator of Tissue Tolerance. Cell 2019;178:1231-1244 e1211
36. Storling J, Juntti-Berggren L, Olivecrona G, Prause MC, Berggren PO, Mandrup-Poulsen T: Apolipoprotein CIII reduces proinflammatory cytokine-induced apoptosis in rat pancreatic islets via the Akt prosurvival pathway. Endocrinology 2011;152:3040-3048
37. Cnop M, Hannaert JC, Hoorens A, Eizirik DL, Pipeleers DG: Inverse relationship between cytotoxicity of free fatty acids in pancreatic islet cells and cellular triglyceride accumulation. Diabetes 2001;50:1771-1777
38. Wei D, Li J, Shen M, Jia W, Chen N, Chen T, Su D, Tian H, Zheng S, Dai Y, Zhao A: Cellular production of n-3 PUFAs and reduction of n-6-to-n-3 ratios in the pancreatic beta-cells and islets enhance insulin secretion and confer protection against cytokine-induced cell death. Diabetes 2010;59:471-478
39. Bi X, Li F, Liu S, Jin Y, Zhang X, Yang T, Dai Y, Li X, Zhao AZ: omega-3 polyunsaturated fatty acids ameliorate type 1 diabetes and autoimmunity. J Clin Invest 2017;127:1757-1771
40. Tersey SA, Bolanis E, Holman TR, Maloney DJ, Nadler JL, Mirmira RG: Minireview: 12-Lipoxygenase and Islet beta-Cell Dysfunction in Diabetes. Mol Endocrinol 2015;29:791-800
41. Lei X, Zhang S, Emani B, Barbour SE, Ramanadham S: A link between endoplasmic reticulum stress-induced beta-cell apoptosis and the group VIA Ca2+-independent phospholipase A2 (iPLA2beta). Diabetes Obes Metab 2010;12 Suppl 2:93-98
42. Ma Z, Ramanadham S, Hu Z, Turk J: Cloning and expression of a group IV cytosolic Ca2+-dependent phospholipase A2 from rat pancreatic islets. Comparison of the

expressed activity with that of an islet group VI cytosolic Ca2+-independent phospholipase A2. Biochim Biophys Acta 1998;1391:384-400
43. Floyel T, Brorsson C, Nielsen LB, Miani M, Bang-Berthelsen CH, Friedrichsen M, Overgaard AJ, Berchtold LA, Wiberg A, Poulsen P, Hansen L, Rosinger S, Boehm BO, Ram R, Nguyen Q, Mehta M, Morahan G, Concannon P, Bergholdt R, Nielsen JH, Reinheckel T, von Herrath M, Vaag A, Eizirik DL, Mortensen HB, Storling J, Pociot F: CTSH regulates beta-cell function and disease progression in newly diagnosed type 1 diabetes patients. Proc Natl Acad Sci U S A 2014;111:10305-10310
44. Wan X, Vomund AN, Peterson OJ, Chervonsky AV, Lichti CF, Unanue ER: The MHC-II peptidome of pancreatic islets identifies key features of autoimmune peptides. Nat Immunol 2020;
45. Fontana P, Bonfiglio JJ, Palazzo L, Bartlett E, Matic I, Ahel I: Serine ADP-ribosylation reversal by the hydrolase ARH3. Elife 2017;6
46. Abplanalp J, Leutert M, Frugier E, Nowak K, Feurer R, Kato J, Kistemaker HVA, Filippov DV, Moss J, Caflisch A, Hottiger MO: Proteomic analyses identify ARH3 as a serine mono-ADP-ribosylhydrolase. Nat Commun 2017;8:2055
47. Mashimo M, Bu X, Aoyama K, Kato J, Ishiwata-Endo H, Stevens LA, Kasamatsu A, Wolfe LA, Toro C, Adams D, Markello T, Gahl WA, Moss J: PARP1 inhibition alleviates injury in ARH3-deficient mice and human cells. JCI Insight 2019;4
48. Burkart V, Wang ZQ, Radons J, Heller B, Herceg Z, Stingl L, Wagner EF, Kolb H: Mice lacking the poly(ADP-ribose) polymerase gene are resistant to pancreatic beta-cell destruction and diabetes development induced by streptozocin. Nat Med 1999;5:314-319
49. Masutani M, Suzuki H, Kamada N, Watanabe M, Ueda O, Nozaki T, Jishage K, Watanabe T, Sugimoto T, Nakagama H, Ochiya T, Sugimura T: Poly(ADP-ribose) polymerase gene disruption conferred mice resistant to streptozotocin-induced diabetes. Proc Natl Acad Sci U S A 1999;96:2301-2304
50. Perez-Riverol Y, Csordas A, Bai J, Bernal-Llinares M, Hewapathirana S, Kundu DJ, Inuganti A, Griss J, Mayer G, Eisenacher M, Perez E, Uszkoreit J, Pfeuffer J, Sachsenberg T, Yilmaz S, Tiwary S, Cox J, Audain E, Walzer M, Jarnuczak AF, Ternent T, Brazma A, Vizcaino JA: The PRIDE database and related tools and resources in 2019: improving support for quantification data. Nucleic Acids Res 2019;47:D442-D450
51. Merico D, Isserlin R, Stueker O, Emili A, Bader GD: Enrichment map: a network-based method for gene-set enrichment visualization and interpretation. PLoS One 2010;5:e13984

Figure 1

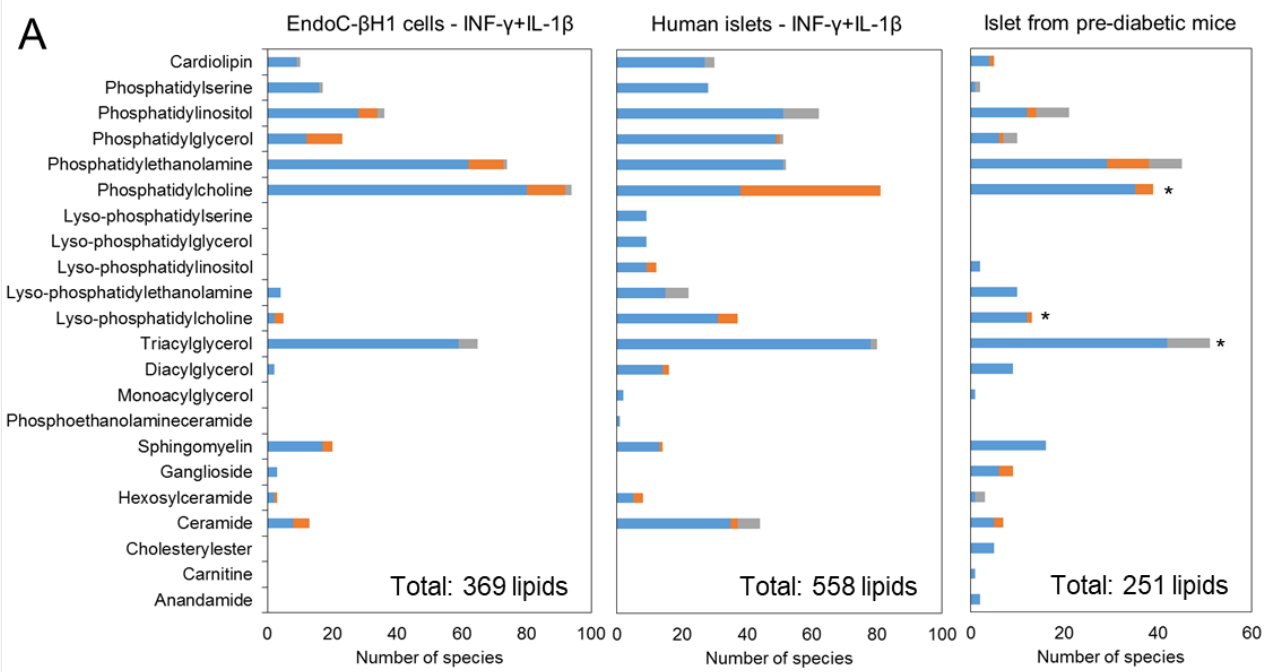

Enriched features		
EndoC-βH1 cells - INF-γ+IL-1β	**Human islets - INF-γ+IL-1β**	**Islet from pre-diabetic mice**
•Phosphatidylglycerol	•Phosphatidylcholine	•Triacylglycerol with total number of carbon 58 in the fatty acid chains
•Plasmanyl-phosphatidylethanolamine	•Phospholipid with C17 fatty acyl chain	
•C20:5 fatty acyl chains	•Phosphatidylglycerol with fatty acyl chain with 3 unsaturations	
•Phosphatidylcholine with total number of carbon 38 in the fatty acid chains	•Phospholipid with 22:5 fatty acyl chain	
•Phospholipid with 6 unsaturations		
•Triacylglycerol with 3 unsaturations		
•Phospholipid with 20:5 fatty acyl chain		
•Phosphatidylcholine with C18:0 fatty acid chains		

Figure 2

	Sample					
Common features	**EndoC-βH1 cells - INF-γ+IL-1β**		**Human islets - INF-γ+IL-1β**		**Islets from pre-diabetic mice**	
	Species	**FC**	**Species**	**FC**	**Species**	**FC**
Increased levels of LysoPC	PC(0:0/16:0)_A	0.91	PC(0:0/16:0)_B	0.27	PC(20:1/0:0)	0.35
	PC(0:0/18:0)	0.72	PC(0:0/18:0)_B	0.24		
	PC(0:0/18:1)_A	0.78	PC(0:0/18:1)_B	0.32		
			PC(17:1/0:0)	0.25		
			PC(17:0/0:0)_B	0.27		
			PC(22:2/0:0)	0.22		
Increased levels of PC with very long, polyunsuaturated fatty acids	PC(16:0/20:5)	0.46	PC(15:0/20:4)	0.29	PC(16:0/22:5);PC(18:1/20:4)	0.60
	PC(18:0/20:3)_B	0.54	PC(15:0/22:6)	0.22	PC(18:1/22:6)	0.87
	PC(18:0/22:3)	0.56	PC(16:0/20:3);PC(18:1/18:2)	0.29	PC(20:2/22:6)	0.59
	PC(18:0/22:6)	0.93	PC(16:0/22:5);PC(18:1/20:4); PC(18:2/20:3)_B	0.53		
	PC(18:1/20:3)_B	0.48	PC(17:0/20:4)	0.24		
	PC(18:1/20:4);PC(16:0/22:5)	0.80	PC(17:0/22:5);PC(19:1/20:4)	0.30		
	PC(18:1/20:5)	0.40	PC(17:1/20:4)	0.17		
			PC(18:0/20:4);PC(18:1/20:3)_B	0.16		
			PC(18:0/22:5)	0.17		
			PC(18:0/22:6)	0.13		
			PC(18:1/20:5);PC(18:2/20:4); PC(16:0/22:6);PC(16:1/22:5)	0.21		
			PC(18:1/22:6);PC(20:3/20:4)	0.14		
			PC(18:2/20:1)	0.22		
			PC(18:2/20:2);PC(18:1/20:3)_A	0.24		
			PC(20:1/20:4);PC(20:2/20:3)	0.23		
			PC(20:2/20:4)	0.32		
			PC(20:3/22:4)	0.33		
			PC(20:4/22:1)	0.14		
			PC(22:4/22:6)	0.36		
Decreased levels of TG	TG(44:1)	-0.87	TG(54:1)	-0.42	TG(52:3)	-0.61
	TG(49:2)	-0.44	TG(56:2)	-0.42	TG(56:3)	-0.67
	TG(49:3)	-0.64			TG(54:3)	-0.47
	TG(50:3)	-0.19			TG(58:6)	-0.91
	TG(51:3)	-0.40			TG(56:4)	-0.77
	TG(53:3)	-0.18			TG(58:8)	-0.68
					TG(52:2)	-0.33
					TG(56:8)	-0.82
					TG(58:9)	-0.75

Log_2(fold change)				
-1.0	-0.5	0.0	0.5	1.0

Figure 3

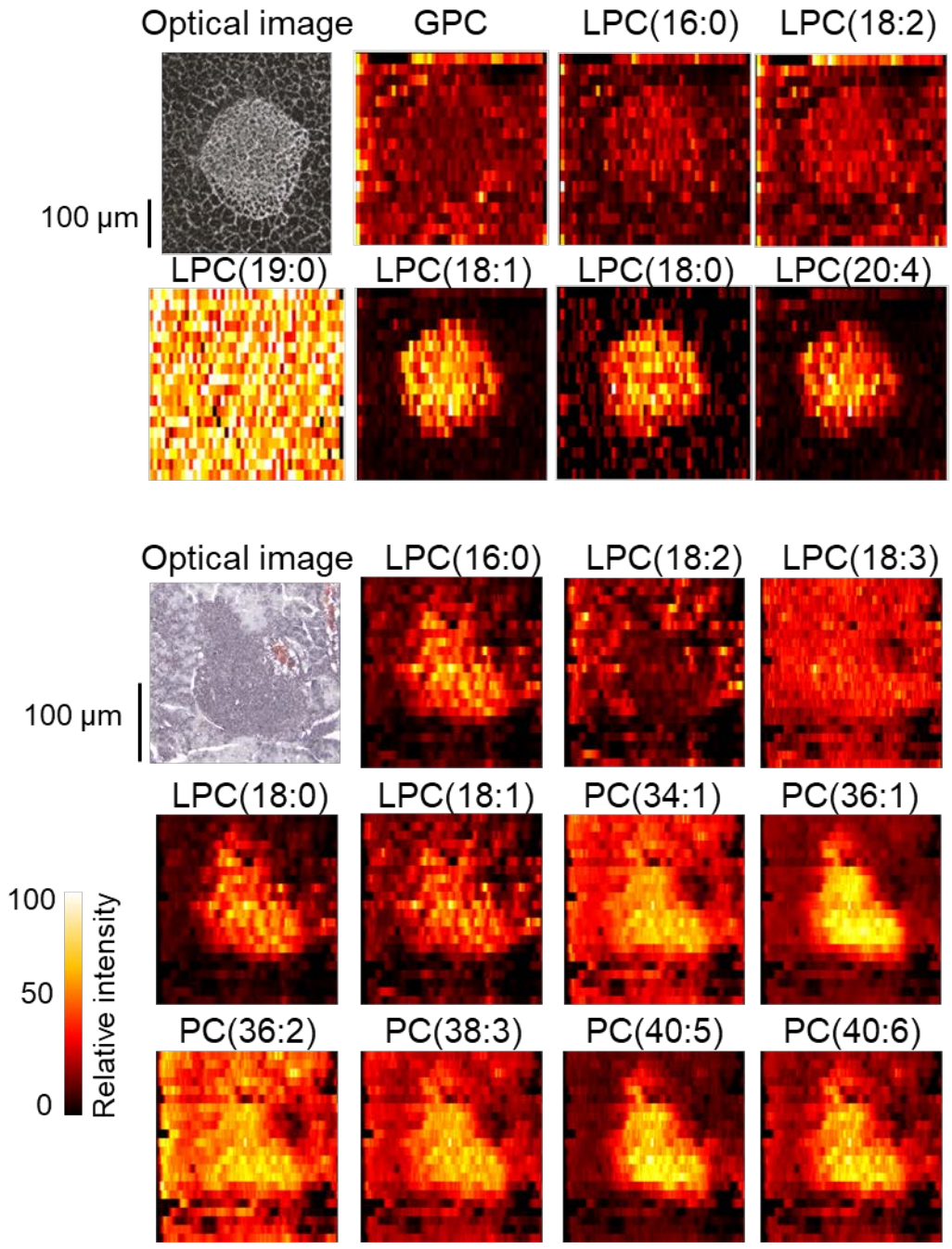

Figure 4

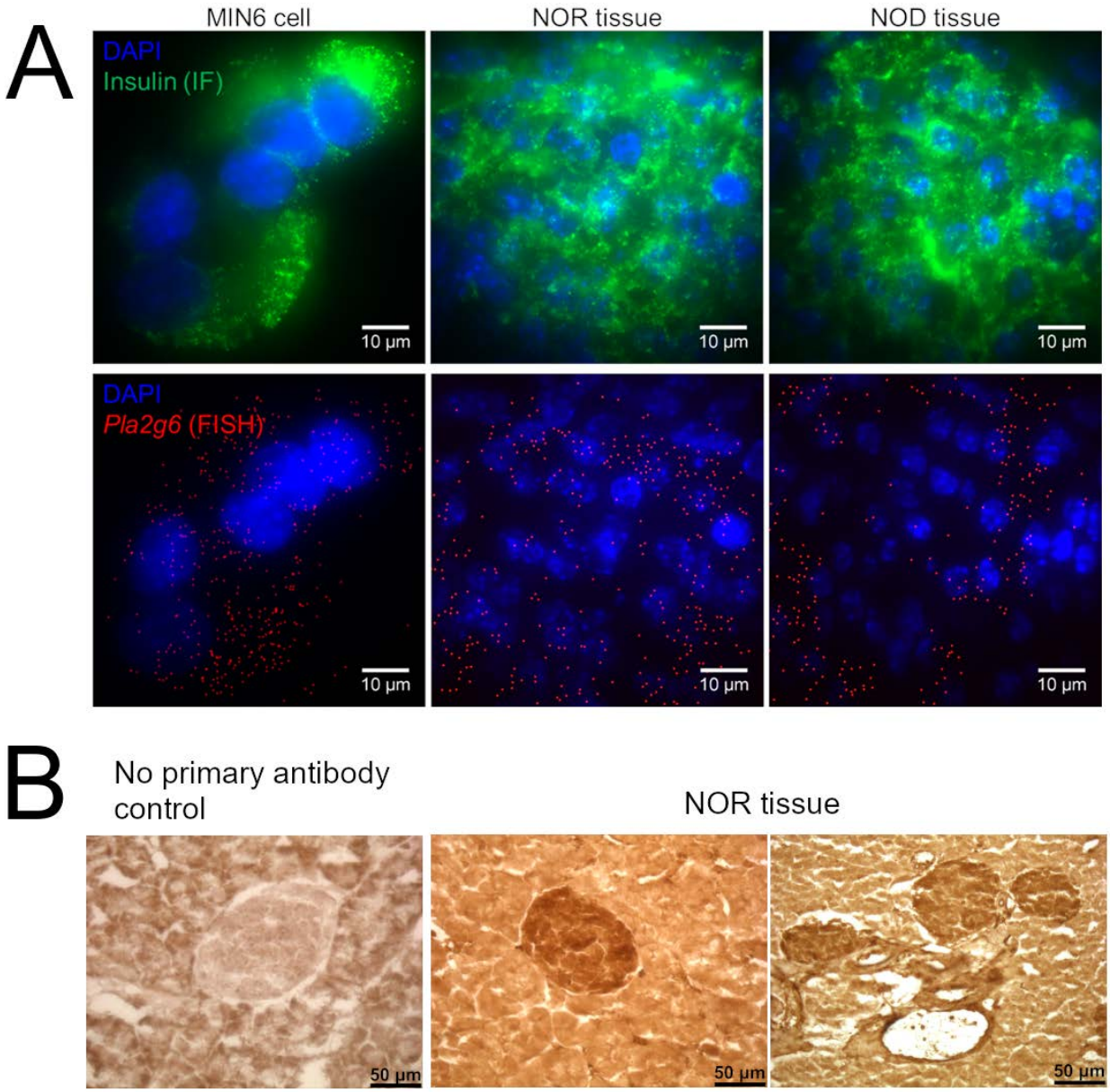

Figure 5

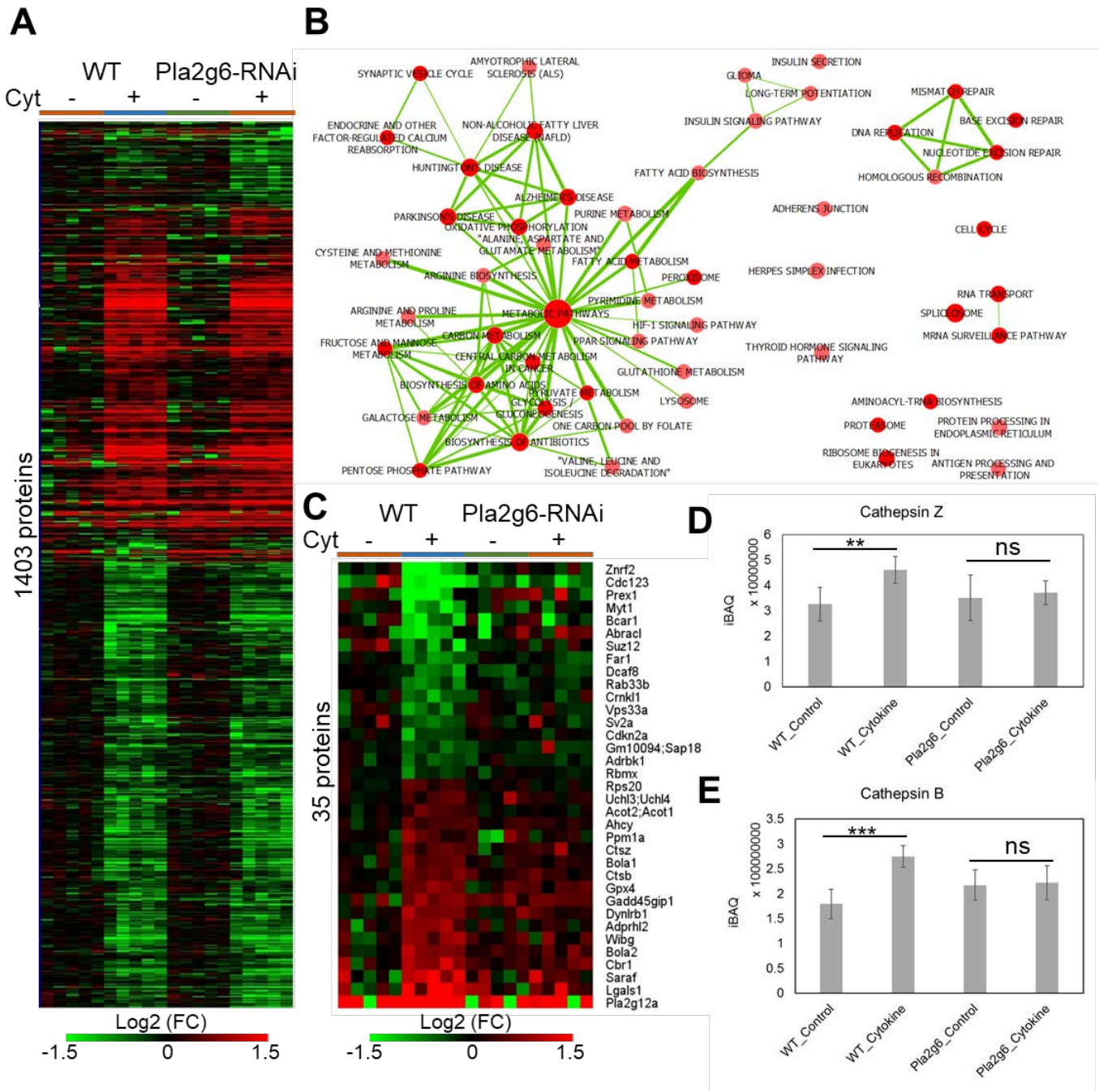

Figure 6